ESTIMATION OF GEOMETRIC TORTUOSITY FOR BULK ACOUSTIC ABSORBERS USING THE HEAT METHOD
2025 Stowe, Vermont

Anthony Ciletti[1] and Bhisham Sharma[2]
Michigan Technological University
1400 Townsend Ave, Houghton, Michigan, 49931-1295

William Schneck[3] and Peter Spaeth[4]
NASA Langley Research Center
Mail Stop 231, Hampton, Virginia, 23681-2199

Martha Brown[5]
NASA Langley Research Center
Mail Stop 164D, Hampton, Virginia, 23681-2199

ABSTRACT

Geometric tortuosity — the ratio of arc length to the straight-line distance between its endpoints — is among the key parameters needed to predict a porous material's acoustic properties. Here, we adapt the heat method, commonly used for surface calculations, to measure tortuosity within the fluid volume of complex three-dimensional porous lattice unit cells of acoustical materials. Our implementation in Python relies on the open-source scikit-fem library to handle finite element operations on a hexahedral mesh of the fluid domain. We apply adiabatic boundary conditions at both the fluid-solid interfaces and the unit cell faces, allowing heat to flow from an inlet face through the fluid domain for a brief period. Poisson's equation is then solved using the resulting temperature gradient field. Tortuosity is evaluated at a discharge face opposite the inlet, and path-lines through the gradient field are visualized. We also generate a histogram and spatial map of tortuosity values on the discharge face, revealing a strong dependence on local geometric features, including through-holes. Overall, our results show that the heat method offers a viable computational alternative to estimating the tortuosity of porous acoustical materials.

---

[1]Graduate Student, Mechanical and Aerospace Engineering

[2]Associate Professor, Mechanical and Aerospace Engineering

[3]Research Engineer, Nondestructive Evaluation Sciences Branch

[4]Senior Research Physicist, Nondestructive Evaluation Sciences Branch

[5]Senior Research Engineer, Aeroacoustics Branch

1. INTRODUCTION

Bulk acoustic absorbers are porous and fibrous materials used as liners for reduced sound reflection within a space or transmission to other spaces. Bulk absorbers have intricate, often anisotropic internal structures. While key to sound absorption, the complexity of the pore space poses significant challenges for characterizing the acoustic behavior. Biot poroelasticity theory models wave propagation in both solid and fluid domains of a porous material [1, 2]. Above a phase decoupling frequency, it can be assumed that the solid phase is not excited by acoustic disturbances [3]. This decoupling frequency is 100 Hz or lower for bulk materials. It is therefore possible to represent a motionless skeleton bulk material as an equivalent fluid with dynamic (frequency-functioned) density and bulk modulus. Researchers have used semi-empirical models like that developed by Johnson [4], Champoux and Allard [5] (the JCA model), and its improvements by Lafarge [6] (JCAL) and Pride [7] (JCALP or JCAPL) to relate these dynamic properties to a set of scalar transport parameters. These transport parameters are solely dependent on the geometry of the pore structure. For instance, the open porosity is the volume fraction of the material available for saturating fluids, and the thermal and viscous characteristic lengths are related to the size of pores and constrictions within the material. In this paper, our focus is the extraction of one particular transport parameter: the high-frequency limit of tortuosity.

Dynamic tortuosity is the ratio between the effective density of equivalent fluid and the density of air. The value as frequency approaches infinity is the high-frequency limit of tortuosity (hereafter referred to simply as tortuosity). There are three primary approaches to estimate tortuosity and the other transport parameters. It is possible to directly measure all the transport parameters used in the JCAL model, with tortuosity being found via ultrasonic testing [8]. Another approach is inverse characterization from an impedance tube measurement: an optimization routine seeks transport parameter values that minimize error between measured and predicted absorption coefficient [9, 10]. Finally, finite element (FE) software can be used to solve simplifications of the governing Navier-Stokes equations. For tortuosity, Laplace's electric conductivity problem is solved through a FE representation of the pore structure (an equivalency exists between this problem and inviscid flow [11]), and tortuosity can be found as an expression involving the electric field [12].

The direct measurement and inverse characterization techniques are limited to the analysis of physical or as-manufactured porous media. The numerical method can only be applied on digital representations of pore structures, and typically also requires periodicity. No contemporary method can analyze both physical and digital geometries, and the aforementioned methods have additional limitations that impact accuracy and versatility. The driving motivation behind this work is to find an alternative that bridges the physical-digital gap. This is especially important for additively manufactured materials. 3D-printing enables the realization of complex, layered, and anisotropic materials for use as sound absorbers [13, 14], but the manufactured geometry does not exactly match the designed topology. Consequently, differences between acoustic performance predicted from designed geometry and measured from manufactured samples have been observed [15].

We investigate the use of an alternative definition of tortuosity from a geometric perspective. The ideal gas law and sound speed equations can be used to show the equivalence of tortuosity to the squared ratio of sound speeds. Given that sound speed is a ratio between the distance traveled and time of propagation, we can express the high-frequency limit of tortuosity, α_∞:

$$\alpha_\infty = \left(\frac{l_{eff}}{l_0}\right)^2 \tag{1}$$

where l_0 is the thickness of the acoustic material along the incident wave direction, and l_{eff} is the length of the tortuous propagation path within the material. Researchers have used pathfinding algorithms to extract paths through the fluid domain of a structure, and calculate the tortuosity of these paths [16, 17]. Others have used simplified skeletal or pore-network representations of the bulk structure and used Dijkstra's or similar methods to generate paths [18, 19]. These pathfinding methods are agnostic to the periodicity or isotropy of the pore structure, and thus can be applied to more structures than the contemporary finite-element process. Further, digital geometries obtained from non-destructive means, such as micro-computed tomography (μCT), can be analyzed. Thus, as-manufactured and as-designed pore structures can be investigated using the same tool.

Calculated tortuosity is highly dependent on the specific path taken. Standard pathfinding algorithms applied to an unmodified pore space often yield routes that cling closely to the walls when navigating through bends, minimizing the overall path length. Consequently, the tortuosity values obtained this way are consistently lower than those estimated using skeletonization or pore-network approaches. Moreover, the precise nature of the actual path relevant to sound propagation in these structures is still unclear. More research is needed to understand sound propagation within the pore space and to adjust these methods to more accurately reflect that behavior.

In this paper, we apply the heat method for distance calculation as an alternative to traditional pathfinding methods, which differentiates itself by the simulation of thermal energy propagation to find tortuous paths through a domain. In Sec. 2, we elaborate on the heat method. In Sec. 3, we describe porous absorber unit cells investigated in this study. The heat method is applied to these structures and Sec. 4 contains the resulting field visualizations and tortuosity distributions. The significance of the findings and future use of the method are discussed in Sec. 5

2. THE HEAT METHOD

Varadhan's formula relates the distance ϕ between two points x_1 and x_2 on a curved domain if the heat kernel k_{t,x_1} is known [20]:

$$\phi(x_1, x_2) = \lim_{t \to 0} \sqrt{-4t log(k_{t,x_1}(x_2))} \tag{2}$$

where t is time. Varadhan's formula can be interpreted as follows: for heat to have diffused from x_1 to x_2 in an arbitrarily small timescale, the diffusion path must have been the shortest possible route. The drawback of this formula is the precise reconstruction of the heat kernel necessary for accurate distance calculations. The heat method captures the intuitive behavior of Varadhan's formula while only requiring a function whose gradient is parallel to the gradient of the true distance field at all points.

The heat method process as outlined by Crane et al. [21] consists of four steps. First, thermal boundary conditions are applied: a nonzero temperature is assigned to the regions from which distance is to be calculated. In our study, we impose this condition on the fluid domain elements located on one of the six face outer faces of the unit cell, hereafter referred to as the inlet face. This approach allows distances to be computed from entire regions rather than from a single point. Second, heat is allowed to propagate throughout the domain for a finite period, resulting in a temperature field. The duration of this propagation period affects the outcome: vanishingly short times yield better approximations of geodesic paths, whereas longer times produce smoothed paths (see Fig. 14 in [21]). Third, the gradient of the resulting temperature field is computed, and the corresponding vector field

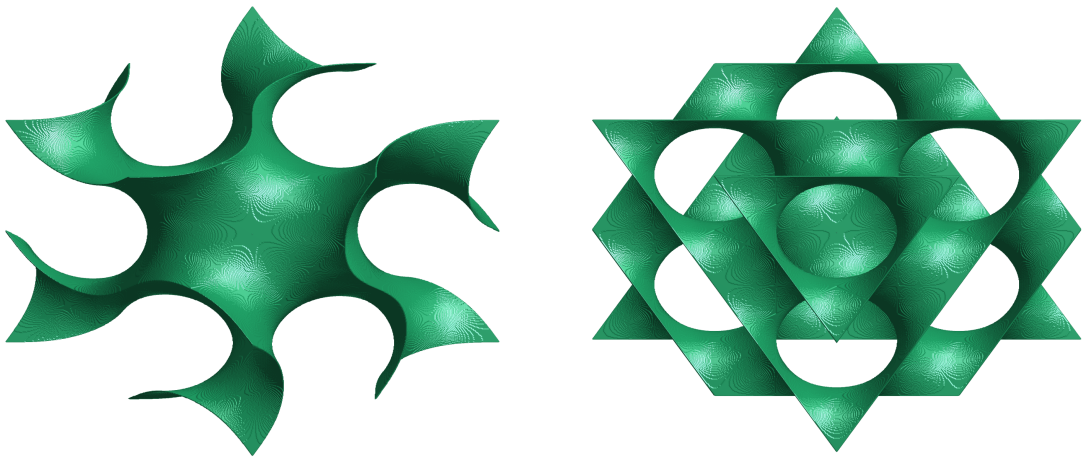

(a) (b)

Figure 1: Gyroid (a) and Diamond (b) TPMS unit cells with no wall thickness.

is normalized such that vector magnitude at all points is unity. This normalization is crucial because the distance calculation is independent of the magnitude of the temperature change; only the direction in which the temperature decreases is relevant. Fourth, Poisson's equation is solved on the normalized vector field F:

$$\nabla^2 \phi = \nabla \cdot F. \tag{3}$$

In other words, the divergence of the normalized vector field F equals the Laplacian of the distance function approximation ϕ, which is a scalar field defined at each point in the domain. In Poisson's equation, F could be any vector field, however in the heat method it is the normalized temperature gradient field found in step three. Crane et al. [21] focused on demonstrations of the heat method on curved surfaces; however, the heat method is not limited to thin domains. In this work, we extend the application of the heat method to a volume, specifically the fluid domain of a porous media.

3. TRIPLY PERIODIC MINIMAL SURFACES

The heat method can be applied to any pore network, whether derived from existing structures or designed anew. In this work, we first investigate triply periodic minimal surfaces (TPMS). It is straightforward to tune the porosity of these structures, which greatly impacts pore space geometry and therefore acoustic performance. TPMS are also generally amenable to additive manufacturing. Moreover, TPMS exhibit attractive properties for multifunctional applications, including (but not limited to) mechanical energy absorption, thermal exchange, use as bioscaffolds, and acoustic energy absorption.

A minimal surface has zero local mean curvature everywhere. Representative unit cells of the TPMS – visualized in Fig. 1 – are repeated in all three Cartesian directions (i.e., triply periodic). Each TPMS is defined by a trigonometric equation. For instance, the Gyroid and Diamond isosurfaces are given by [22]:

$$f_G = \sin(x)\cos(y) + \sin(y)\cos(z) + \sin(z)\cos(x) - c_G, \tag{4}$$

$$\begin{aligned} f_D = {} & \sin(x)\sin(y)\sin(z) + \sin(x)\cos(y)\cos(z) \\ & + \cos(x)\sin(y)\cos(z) + \cos(x)\cos(y)\sin(z) - c_D. \end{aligned} \tag{5}$$

To achieve a desired porosity, the isosurface is thickened by subtracting a scalar c (i.e., c_G or c_D), computed as a function of the desired porosity θ:

$$c_G = 3(\theta - 0.5), \tag{6}$$

$$c_D = 1.5177\theta^5 - 3.7941\theta^4 + 4.3168\theta^3 - 2.6810\theta^2 + 3.2014\theta - 1.2803. \tag{7}$$

In this study, we use a Gyroid unit cell at 50% porosity, as well as Diamond unit cells designed with porosities of 40%, 50% and 60%.

Each unit cell's fluid phase is represented by a regular hexahedron mesh with a side length equal to $\frac{1}{50}$ of the overall unit cell's length. An element in the $50 \times 50 \times 50$ grid is included if the function f_D from Eqn. 4 or Eqn. 5, evaluated at the element's centroid, is negative. This approach is analogous to a stack of images, the format used by μCT data. Since binarized μCT data can be easily converted to this format, it can be analyzed using the same method, mesh format, and mesh size as digitally constructed unit cells. Consequently, comparisons between as-designed and as-manufactured materials are possible with minimal meshing-induced differences. In preparation for future research on these comparisons, we have chosen this meshing approach over traditional tetrahedral elements.

This unit cell construction and meshing process is implemented in Python with the assistance of the VTK package [23]. The generated hexahedron meshes are then used in the heat method of Sec. 2, which is made possible by the scikit-fem package [24]. Paraview [25] visualizations give insight into the nature of the resulting distance fields.

4. RESULTS

Gyroid (left) and Diamond (right) TPMS unit cells designed to 50% porosity are shown in Fig. 2. In these figures and all following unit cell representations, the inlet is the top face of the sample, and the discharge face is the bottom (being directly opposite to the inlet). Each voxel in the fluid domain is translucent and is colored based on the tortuous distance from any voxel on the inlet face, normalized to the unit cell length. The same color scale is used for isosurfaces of tortuous distance, representing distances of one-third, two-thirds, and the full length of the unit cell, as well as for paths seeded through the fluid domain. These paths follow the gradient of the distance field, with starting points randomly seeded across the inlet face. There is a clear distinction between paths extracted using traditional pathfinding algorithms and the seeded paths illustrated in Fig. 2. Conventional algorithms tend to produce paths that cling closely to the fluid–solid interfaces to minimize the distance. In contrast, the seeded paths of Fig. 2 generally run parallel to the nearest fluid–solid boundary while still advancing toward the discharge region. This behavior is also evident in the distance isosurfaces which, near the inlet, appear nearly normal to the axes of the fluid network's throats.

The discharge face of the unit cells along with a histogram of the distance values for all voxels on that face are displayed in Fig. 3. Because the discharge face is one unit cell length away from the inlet face, these distance values directly represent the dimentionless geometric tortuosity (with the denominator in Eqn. 1 equal to unity). Comparing Fig. 3 with the geometry in Fig. 2 reveals that

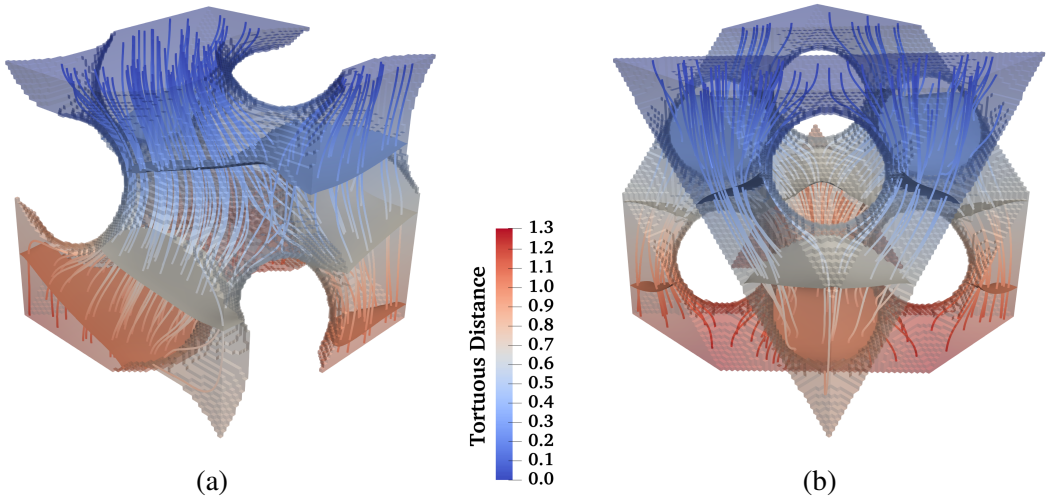

Figure 2: Paraview visualizations of the distance field for the Gyroid (a) and Diamond (b) unit cells at 50% porosity, including voxel shading, distance isosurfaces, and gradient-following paths.

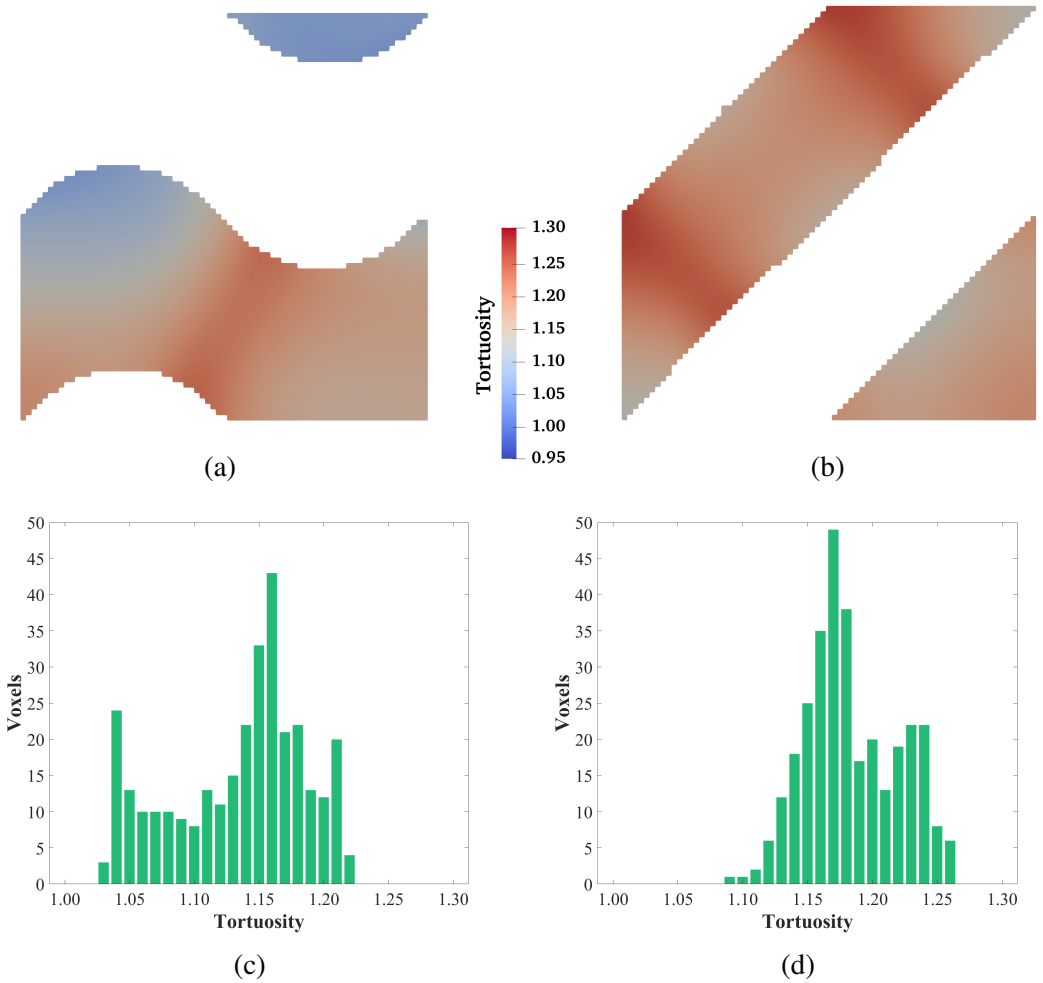

Figure 3: The visualizations and histograms of tortuosity on the Gyroid ((a) and (c)) and Diamond ((b) and (d)) 50% porosity unit cell discharge faces.

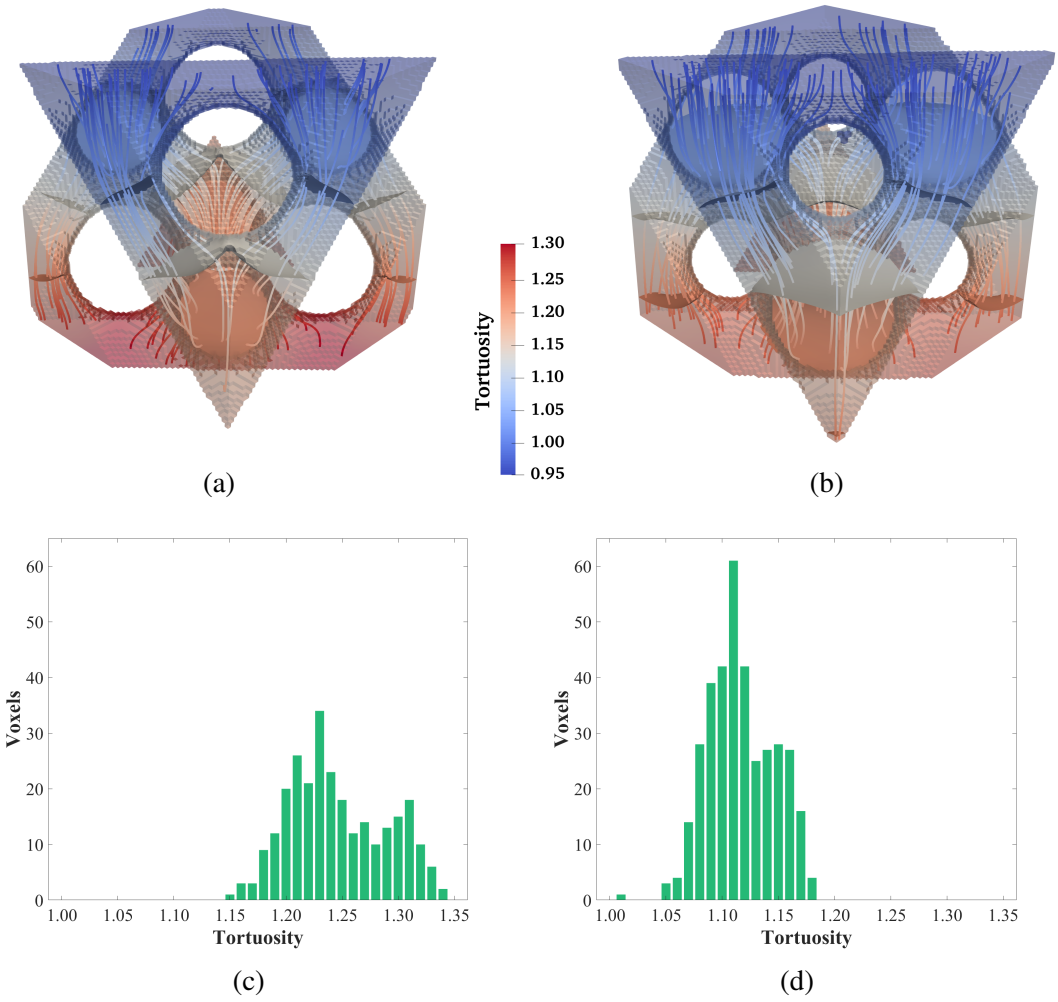

Figure 4: Visualizations and discharge face tortuosity histograms for the Diamond 40% ((a) and (c)) and 60% ((d) and (b)) porosity unit cells.

regions exhibiting the highest tortuosity values lie directly beneath large solid features, necessitating longer travel distances for the paths reaching these voxels.

The histogram shows that the tortuosity distribution spans from 1.03 to 1.22 for the Gyroid unit cell and from 1.09 to 1.26 for the Diamond unit cell. Since the JCA, JCAL, and JCALP models require a single scalar value for the tortuosity transport parameter, synthesizing the per-voxel tortuosity distribution into a representative per-structure value (for instance, the square mean or median) may be appropriate. Future research is needed to identify the most suitable metric, possibly through comparisons with values obtained via direct measurement or inverse techniques.

The effect of porosity modification is illustrated via 3D visualizations and discharge face tortuosity histograms in Fig. 4. As porosity decreases, the histogram shifts toward higher tortuosity values. This is also evident from the distance isosurfaces, which move closer to the inlet face and to each other as porosity decreases. Inverse proportionality between porosity and tortuosity is commonly observed in bulk materials.

Lastly, we observe the impact of altering the time-scale in step two of the heat method. As noted by Crane et al. [21], shorter time periods yield paths closer to the true geodesic, resulting in lower

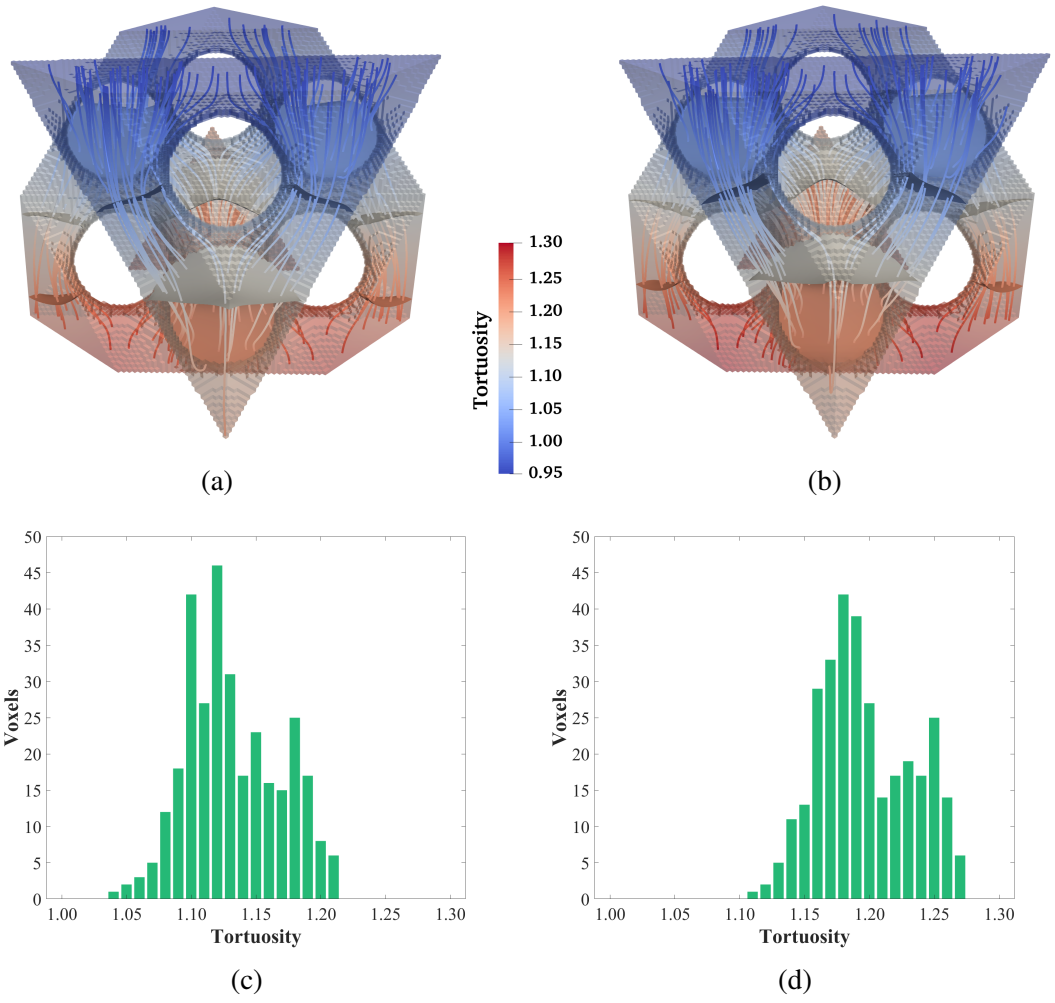

Figure 5: Visualizations ((a) and (b)) and discharge face tortuosity histograms ((c) and (d)) for the Diamond 50% when using thermal propagation time periods of 1/10 ((a) and (c)) and 10 times ((b) and (d)) that of Fig. 2.

tortuosity values. This behavior is evident in Fig. 5, which shows results for a timescale one-tenth (left) and ten times (right) that of the 50% porosity Diamond unit cell in Fig. 2. Note that the four faces parallel to the propagation direction do not have a periodic boundary condition; instead, they use the same conditions as the fluid–solid interfaces. While this choice has minimal effect in the analysis of a larger bulk material composed of many unit cells, it could impact the analysis of a single unit cell. Further investigation into the implementation of these boundary conditions is needed to fully understand their effects.

5. CONCLUSIONS

The heat method was applied to TPMS unit cells to extract and visualize geometric tortuosity at the discharge face. Consistent with previous research, as unit cell porosity decreased, the tortuosity distribution shifted to higher values. Similarly, as Crane et al. [21] noted, longer thermal propagation times resulted in higher tortuosity.

Further development is required, including the extraction of a single representative tortuosity metric and implementation of periodic boundary conditions. Clarification is also needed regarding the relationship between acoustic and geometric tortuosity. Specifically, do acoustic disturbances follow the most efficient paths as suggested by pathfinding algorithms, or do they take more natural routes akin to those observed here or derived via pore skeletonization? How do geometric details such as dead-end pores or rough surfaces impact acoustic wave propagation? A deeper understanding of these issues would help determine which geometric approach best approximates actual behavior.

Overall, the heat method is a promising alternative for extracting geometric tortuosity. The distribution of tortuosity values at the discharge region provides insight to the path differences within the unit cell previously unseen. The method can be applied to as-designed and as-manufactured geometries, an important capability if the impact of manufacturing defects is germane. The dependence of path behavior on time-step selection can be leveraged by future research. A parametric study of the time-step values comparing computed tortuosity values with direct measurements could be performed, with results that align best potentially indicating the gradient field most accurate to the true nature of acoustic propagation paths.

ACKNOWLEDGMENTS

The following acknowledgments are for consecutive, non-overlapping funding sources. This material is based upon work supported by the National Science Foundation Graduate Research Fellowship Program under Grant no. 2437847. Any opinions, findings, and conclusions or recommendations expressed in this material are those of the author(s) and do not necessarily reflect the views of the National Science Foundation. Anthony Ciletti would also like to acknowledge funding support from the Advanced Air Transport Technologies Project of the NASA Advanced Air Vehicles Program.

REFERENCES

[1] M. A. Biot. Theory of propagation of elastic waves in a fluid-saturated porous solid. I. Low-frequency range. *The Journal of the Acoustical Society of America*, 28(2):168–178, March 1956.

[2] M. A. Biot. Theory of propagation of elastic waves in a fluid-saturated porous solid. II. Higher frequency range. *The Journal of the Acoustical Society of America*, 28(2):179–191, March 1956.

[3] C. Zwikker and C. W. Kosten. *Sound Absorbing Materials*. Elsevier Publishing Company, 1949. Google-Books-ID: AkghAAAAMAAJ.

[4] D. L. Johnson, J. Koplik, and R. Dashen. Theory of dynamic permeability and tortuosity in fluid-saturated porous media. *Journal of Fluid Mechanics*, 176:379–402, March 1987.

[5] Y. Champoux and J. F. Allard. Dynamic tortuosity and bulk modulus in air-saturated porous media. *Journal of Applied Physics*, 70(4):1975–1979, August 1991.

[6] D. Lafarge, P. Lemarinier, J. F. Allard, and V. Tarnow. Dynamic compressibility of air in porous structures at audible frequencies. *The Journal of the Acoustical Society of America*, 102(4):1995–2006, October 1997.

[7] S. R. Pride, F. D. Morgan, and A. F. Gangi. Drag forces of porous-medium acoustics. *Physical Review B*, 47(9):4964–4978, March 1993. Publisher: American Physical Society.

[8] J. F. Allard, B. Castagnede, M. Henry, and W. Lauriks. Evaluation of tortuosity in acoustic porous materials saturated by air. *Review of Scientific Instruments*, 65(3):754–755, March 1994.

[9] R. Panneton and X. Olny. Acoustical determination of the parameters governing viscous dissipation in porous media. *The Journal of the Acoustical Society of America*, 119(4):2027–2040, April 2006.

[10] X. Olny and R. Panneton. Acoustical determination of the parameters governing thermal dissipation in porous media. *The Journal of the Acoustical Society of America*, 123(2):814–824, February 2008.

[11] M. Avellaneda and S. Torquato. Rigorous link between fluid permeability, electrical conductivity, and relaxation times for transport in porous media. *Physics of Fluids A: Fluid Dynamics*, 3(11):2529–2540, November 1991.

[12] T. G. Zieliński. Microstructure-based calculations and experimental results for sound absorbing porous layers of randomly packed rigid spherical beads. *Journal of Applied Physics*, 116(3):034905, July 2014.

[13] B. Wojciechowski, Y. Xue, A. Rabbani, J. S. Bolton, and B. Sharma. Additively manufactured spinodoid sound absorbers. *Additive Manufacturing*, 71:103608, June 2023.

[14] W. Johnston, J. Godakawela, C. Gatti, S. Keshavanarayana, and B. Sharma. Fibro-porous materials: 3D-printed hybrid porous materials for multifunctional applications. *Additive Manufacturing*, 94:104470, August 2024.

[15] A. Lomte and B. Sharma. Effect of geometrical defects on the acoustical transport properties of periodic porous absorbers manufactured using stereolithography. *Noise Control Engineering Journal*, 71(5):365–371, September 2023.

[16] S. J. Cooper, A. Bertei, P. R. Shearing, J. A. Kilner, and N. P. Brandon. TauFactor: An open-source application for calculating tortuosity factors from tomographic data. *SoftwareX*, 5:203–210, 2016.

[17] J. Ávila, J. Pagalo, and M. Espinoza-Andaluz. Evaluation of geometric tortuosity for 3D digitally generated porous media considering the pore size distribution and the A-star algorithm. *Scientific Reports*, 12(1):19463, November 2022.

[18] N. O. Shanti, V. W. L. Chan, S. R. Stock, F. De Carlo, K. Thornton, and K. T. Faber. X-ray micro-computed tomography and tortuosity calculations of percolating pore networks. *Acta Materialia*, 71:126–135, June 2014.

[19] R. Nemati, J. Rahbar Shahrouzi, and R. Alizadeh. A stochastic approach for predicting tortuosity in porous media via pore network modeling. *Computers and Geotechnics*, 120:103406, April 2020.

[20] S. R. S. Varadhan. On the behavior of the fundamental solution of the heat equation with variable coefficients. *Communications on Pure and Applied Mathematics*, 20(2):431–455, 1967.

[21] K. Crane, C. Weischedel, and M. Wardetzky. The heat method for distance computation. *Communications of the ACM*, October 2017. Publisher: ACMPUB27 New York, NY, USA.

[22] J. Feng, J. Fu, X. Yao, and Y. He. Triply periodic minimal surface (TPMS) porous structures: from multi-scale design, precise additive manufacturing to multidisciplinary applications. *International Journal of Extreme Manufacturing*, 4(2):022001, March 2022. Publisher: IOP Publishing.

[23] W. Schroeder, K. Martin, and B. Lorenson. *The Visualization Toolkit*. Kitware, Inc, 4 edition, 2004.

[24] T. Gustafsson and G. D. Mcbain. scikit-fem: A Python package for finite element assembly. *Journal of Open Source Software*, 5(52):2369, August 2020. Publisher: Open Journals.

[25] U. Ayachit. *The ParaView Guide: A Parallel Visualization Application | Guide books | ACM Digital Library*. Kitware, Inc, Clifton Park, New York, January 2015.